Quantum correlations across a metallic screen

M. Al-Amri
Department of Physics, University of York, Heslington, York YO10 5DD, England
and Department of Physics, King Khalid University, Abha, Saudi Arabia

M. Babiker
Department of Physics, University of York, Heslington, York YO10 5DD, England
(Received 17 December 2002; published 29 April 2003)

We show that an optical multilayer system comprising a thin metallic film sandwiched between two different half-space dielectrics generates remarkable quantum correlations for dipole emitters embedded in the structure, both in the far zone and in the near zone. For a pair of such dipole emitters localized in the same region of the structure, the correlations display super-radiance and subradiance phenomena, but the system allows for an unusual and seldom considered scenario in which the emitters are located on different sides and so they are separated by the metallic screen. We explore the quantum correlations in this situation and find that they are sensitive to the type of metallic screen as well as dipole orientation and dielectric mismatch across the screen. We point out the high-symmetry features and attribute the underlying physics to a subtle interplay between image and screening effects in the presence of dielectric mismatch.

DOI: 10.1103/PhysRevA.67.043820 PACS number(s): 42.50.Ct, 34.50.Dy, 32.80.−t, 41.20.Jb

I. INTRODUCTION

There has recently been much effort devoted to seeking means for controlling the properties of the electromagnetic field and matter and, hence, harnessing their interactions in the context of dielectric cavities, particularly in the nanoscale regime [1]. One of the main goals of studies in this area is achieving a desirable improvement in the performance of optoelectronic devices. Other important goals that are currently being vigorously pursued, in terms of modifications of field-matter interactions due to confinement [2], are quantum-information processing and, ultimately, the realization of quantum computing [3–5]. The physics of quantum systems in situations where the electromagnetic-field properties have been modified due to the presence of boundaries now goes under the generic name of cavity quantum electrodynamics [6–17]. When the typical cavity dimensions are in the nanometer to micrometer scale and so are smaller or comparable to an optical dipole transition wavelength, most of the familiar quantum phenomena are liable to change. For instance, spontaneous emission can be drastically reduced or enhanced and it can even be completely suppressed [17].

The simplest system exhibiting cavity effects is the one in which real space is divided into two half spaces, one half space is occupied by a perfect conductor, which excludes all electromagnetic fields of all frequencies, however high, from its interior; while the other half space is occupied by vacuo [18]. An excited electric dipole emitter on the vacuum side in the vicinity of the surface shows evidence of correlation between the dipole and its image in the conductor [19]. Two-dipole correlations have also been investigated in the presence of a perfect conductor half space [20] and the problem can be generalized to an ensemble of electric dipoles cooperatively participating in the emission process [21]. Image effects feature prominently under these circumstances.

Recent work on the dielectric aspects of cavity quantum electrodynamics highlighted the effects of periodicity in semiconductor layered structures [22] and in a set of metallic films immersed in a dielectric [23]. The case of a single metallic film deposited on a thick dielectric slab and so separating it from another similar dielectric slab [24] was also considered. One of the applications of such a structure is in atomic mirrors [25], but the presence of the metallic film makes the structure capable of supporting surface modes, which leads to a strong coupling to quantum systems in the near zone. It turns out that the more general scenario in which the two half spaces have different dielectric constants presents a much richer set of physical phenomena which are the subject of this paper. In particular, the participation of the full set of allowed modes is essential for a general description, including evanescent and propagating modes as well as interface modes. This enables consideration of both the near zone that is dominated by the interface modes and the far-zone that is dominated by the remaining set of modes. The treatment also permits a number of useful limits to be taken and so allowing known results to be recovered. This provides useful checks of the correctness of the results in the general case.

The paper is organized as follows. In Sec. II, we consider energy relaxation of excited states for a single dipole emitter and for a system of two such emitters in unbounded dielectric space. In Sec. III, we discuss the situation in the vicinity of a perfect mirror in the form of a perfect conductor half space. The results of these two sections enable useful comparisons to be made with the results of the more general dielectric system considered in the subsequent sections. In Sec. IV, we describe the asymmetric dielectric structure comprising two semi-infinite dielectric layers separated by a thin metallic sheet of finite conductivity (henceforth, and for reasons which will become clear, to be referred to as the metallic screen). We describe the procedure for quantizing the electromagnetic modes supported by this structure conforming with the electromagnetic boundary conditions at the metallic screen, which include the effects of the finite conductivity. The procedure for determining the modes turns out to be quite cumbersome, despite the apparent simplicity of the

system. In Sec. V, we consider the coupling of the modes to a single dipole emitter localized on either side of the metallic screen and investigate the variations of the relaxation rate with the dielectric constants, the metallic areal electron density, the dipole orientation, and the dipole position relative to the metallic screen. Correlations between the dipole and its image are pointed out and discussed. In Sec. VI, we discuss pair correlations involving cooperative effects exhibited by two such dipole emitters embedded in the structure and which can be located on the same side or on different sides of the metallic screen. Here too the dependence on the various parameters mentioned above reveals interesting features and the theory permits various useful limits to be recovered. In particular, we explore the results of the theory in the large electron-density limit, corresponding to the perfect conductor film case, and the pure half-space dielectric layer structure, corresponding to where the electron density is low. Another limit of interest emerging from the result is that of large distance from the interface which corresponds to unbounded dielectric space. Section VII contains our comments and final conclusions.

II. CORRELATIONS IN UNBOUNDED DIELECTRIC

A. Isolated dipole emitter

In unbounded space occupied by a homogeneous lossless dielectric with a given dielectric constant $\varepsilon(\omega)$ an excited electric dipole active quantum system (for example, a localized atom or molecule, or a quantum dot; henceforth referred to as a dipole emitter) spontaneously discharges its excitation energy by decaying to a lower-energy state. Assuming that the excited ''initial'' state, denoted by $|i\rangle$, has energy $\hbar\omega_i$, the rate at which energy is discharged to the lower state of energy $\hbar\omega_f$, denoted by $|f\rangle$, to lowest order, is given by Fermi's golden rule

$$\tilde{\Gamma}_0=\frac{2\pi}{\hbar^2}\sum_Q |\langle i,\{0\}|H_{int}|f,\{Q\}\rangle|^2\delta(\omega_{if}-\omega_Q), \qquad (1)$$

where $\omega_{if}=\omega_i-\omega_f$ is the transition frequency and $\{Q\}$ is a shorthand for a single-mode electromagnetic-field state of energy $\hbar\omega_Q$, while $\{0\}$ denotes the electromagnetic vacuum state. H_{int} is the interaction of the dipole emitter with the quantized electromagnetic field,

$$H_{int}=-\boldsymbol{\mu}\cdot\mathbf{E}(\mathbf{r},t), \qquad (2)$$

where $\boldsymbol{\mu}$ is the emitter electric dipole moment vector and $\mathbf{E}$ is the quantized electric field which can be written as

$$\mathbf{E}(\mathbf{r},t)=\sum_Q [\tilde{\boldsymbol{\mathcal{E}}}(\mathbf{r},t,Q)a_Q+\text{H.c.}], \qquad (3)$$

where $\tilde{\boldsymbol{\mathcal{E}}}(\mathbf{r},t,Q)$ is the electromagnetic-field distribution function of mode Q and a_Q is its boson annihilation operator. H.c. stands for ''Hermitian conjugate.'' The quantization procedure in a dielectric of volume V is straightforward and amounts to the requirement that the electric-field function for a mode Q is such that the electromagnetic-field energy (which is twice the electric-field energy) satisfies the normalization condition

$$\varepsilon_0\varepsilon\int_V \tilde{\boldsymbol{\mathcal{E}}}(\mathbf{r},t,Q)\cdot\tilde{\boldsymbol{\mathcal{E}}}^*(\mathbf{r},t,Q)d^3\mathbf{r}=\frac{1}{2}\hbar\omega_Q. \qquad (4)$$

In unbounded space the mode functions $\tilde{\boldsymbol{\mathcal{E}}}(\mathbf{r},t,Q)$ are transverse plane waves characterized by two orthogonal polarizations $\hat{\mathbf{e}}_\xi$, $\xi=1,2$. The mode label Q in this case stands for $(\mathbf{k},\xi)$, where $\mathbf{k}$ is the wave vector (orthogonal to both $\hat{\mathbf{e}}_1$ and $\hat{\mathbf{e}}_2$), such that $k^2=\omega^2\varepsilon/c^2$. We have

$$\tilde{\boldsymbol{\mathcal{E}}}(\mathbf{r},t,\mathbf{k},\xi)=i\left(\frac{\hbar\omega}{2\varepsilon_0\varepsilon V}\right)^{1/2}\hat{\mathbf{e}}_\xi e^{i(\mathbf{k}\cdot\mathbf{r}-\omega t)}. \qquad (5)$$

For a single dipole emitter, the final state is the ground state, i.e., $|f\rangle\equiv|g\rangle$ and the initial state is the excited state, i.e., $|i\rangle\equiv|e\rangle$. The dipole matrix element is $\langle\boldsymbol{\mu}\rangle\equiv\langle e|\boldsymbol{\mu}|g\rangle$ and the transition frequency is $\omega_{if}\equiv\omega_0=\omega_e-\omega_g$. On substitution in Eq. (1), we obtain

$$\tilde{\Gamma}_0=\frac{\langle\mu\rangle^2\omega_0^3}{3\pi\hbar\varepsilon_0 c^3}\sqrt{\varepsilon(\omega_0)} \qquad (6)$$

and we note the dependence of the spontaneous rate on the square root of the dielectric constant. This dependence, however, must be supplemented by a local-field correction. Following the model by Glauber and Lewinstein [26,27], we have

$$\Gamma_0=\tilde{\Gamma}_0\mathcal{R}(\omega_0), \qquad (7)$$

where

$$\mathcal{R}=\left(\frac{3\varepsilon(\omega)}{2\varepsilon(\omega)+1}\right)^2. \qquad (8)$$

In free space we have $\mathcal{R}=1$ and the result is the same as $\tilde{\Gamma}_0$. An alternative treatment of the local-field corrections makes use of the virtual cavity model. For details the reader is referred to the articles by de Vries and Lagendijk [28] and Juzeleunas and Andrews [29]. The local-field correction can conveniently be incorporated in the mode function simply by defining the effective electric-field functions $\boldsymbol{\mathcal{E}}(\mathbf{r},t,\mathbf{k},\xi)$ as follows:

$$\boldsymbol{\mathcal{E}}(\mathbf{r},t,\mathbf{k},\xi)=i\left(\frac{\hbar\omega\mathcal{R}}{2\varepsilon_0\varepsilon V}\right)^{1/2}\hat{\mathbf{e}}_\xi e^{i(\mathbf{k}\cdot\mathbf{r}-\omega t)}. \qquad (9)$$

Clearly, use of these mode functions leads directly to the result in Eq. (7).

B. Pair correlations

Pair correlations in an unbounded dielectric involve two identical dipole emitters, labeled 1 and 2 and localized at the space points $\mathbf{r}_1$ and $\mathbf{r}_2$ [30,31]. The lowest excited-state energy of the pair is $\hbar(\omega_e+\omega_g)$ corresponding to the state in

which one of the emitters is in state $|e\rangle$ and the other in state $|g\rangle$. Quantum mechanics stipulates that this level is doubly degenerate and is spanned by two independent states, namely, the symmetric state $|e_+\rangle$ and the antisymmeteric state $|e_-\rangle$ in the form

$$|e_\pm\rangle = \frac{1}{\sqrt{2}}(|e_1 g_2\rangle \pm |g_1 e_2\rangle). \tag{10}$$

The final (ground) state, on the other hand, is singlet and has energy $2\hbar\omega_g$. It is

$$|f\rangle = |g_1 g_2\rangle. \tag{11}$$

Both emitters interact with the same quantized field at their locations $\mathbf{r}_1$ and $\mathbf{r}_2$. The interaction Hamiltonian is [32–34]

$$H_{int} = -\boldsymbol{\mu}_1 \cdot \mathbf{E}(\mathbf{r}_1, t) - \boldsymbol{\mu}_2 \cdot \mathbf{E}(\mathbf{r}_2, t). \tag{12}$$

The rates of deexcitation corresponding to the pair states $|e_\pm\rangle$ are functions of $\mathbf{r}_1$ and $\mathbf{r}_2$ and are given by

$$\Gamma^{\pm}(\mathbf{r}_1, \mathbf{r}_2) = \frac{2\pi}{\hbar^2} \sum_Q |\langle e_\pm, \{0\}|H_{int}|f, \{Q\}\rangle|^2 \delta(\omega_{if} - \omega_Q). \tag{13}$$

The transition frequency in both cases is ω_{if} which is, as before, equal to $\omega_0 \equiv \omega_e - \omega_g$. The quantised electric field is as given in Sec. II A, with the mode functions given by Eq. (9). The evaluation is straightforward and leads to a result for arbitrary dipole orientation

$$\Gamma^{\pm}(\mathbf{r}_1, \mathbf{r}_2) = \Gamma_0 \left\{ 1 \pm \frac{3}{2} \sum_{i,j} \hat{\mu}_i^{(1)} \hat{\mu}_j^{(2)} \mathcal{J}_{ij}(\mathbf{r}_1, \mathbf{r}_2) \right\}, \tag{14}$$

where $\hat{\mu}_i^{(1)}$ and $\hat{\mu}_j^{(2)}$ are the ith and jth Cartesian vector components of unit vectors in the direction of the dipole moments of emitters 1 and 2, respectively. The functions $\mathcal{J}_{ij}$ are in fact functions of the separation between the emitters and can be explicitly written in the following form:

$$\mathcal{J}_{ij}(R) = \alpha_{ij} \frac{\sin\{k_0 R\}}{k_0 R} + \beta_{ij} \left\{ \frac{\cos\{k_0 R\}}{(k_0 R)^2} - \frac{\sin\{k_0 R\}}{(k_0 R)^3} \right\}. \tag{15}$$

Here $k_0 = \omega_0 / c$, $R = |\mathbf{r}_1 - \mathbf{r}_2|$ is the separation vector and α_{ij} and β_{ij} are in the form

$$\alpha_{ij} = \delta_{ij} - \hat{\mathbf{R}}_i \hat{\mathbf{R}}_j, \quad \beta_{ij} = \delta_{ij} - 3\hat{\mathbf{R}}_i \hat{\mathbf{R}}_j, \tag{16}$$

where $\hat{\mathbf{R}}_i$ is the ith Cartesian component of the unit vector $\hat{\mathbf{R}} = \mathbf{R}/R$.

It is interesting to note at this stage that is the small separation limit in which $k_0 R \ll 1$, i.e., $R \ll \lambda/2\pi$, where λ is the dipole transition wavelength, the set of functions $\mathcal{J}_{ij}$ become as follows:

$$\mathcal{J}_{ij} \to \alpha_{ij} - \frac{1}{3}\beta_{ij}. \tag{17}$$

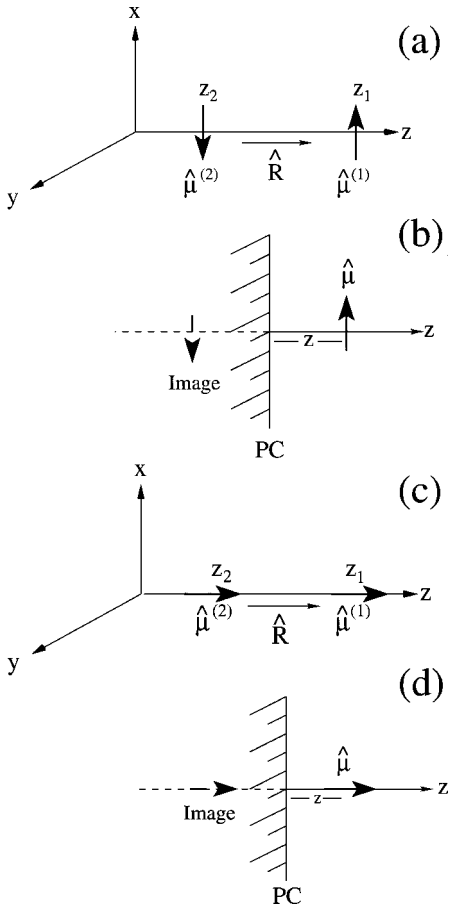

FIG. 1. Schematic figures showing two real dipole emitters in free space (a) and (c) and one dipole and its image in a perfect conductor (b) and (c). The perfect conductor is referred to as PC in the figure. The orientation of the real dipole in (a) and (c) have been chosen to coincide with those of the single dipole and its image in (b) and (d), respectively.

The general result in Eq. (14) has some interesting special cases and limits. In particular, consider the case in which the dipoles are parallel to each other and are both perpendicular to the separation vector **R**. Without loss of generality we take **R** along the z axis, dipole 1 along the positive x axis, and dipole 2 along the negative x axis. This corresponds to the choice $\hat{\mathbf{R}} = (0,0,1)$; $\hat{\boldsymbol{\mu}}^{(1)} = (1,0,0)$, and $\hat{\boldsymbol{\mu}}^{(2)} = (-1,0,0)$, as shown schematically in Fig. 1(a). We then have

$$\sum_{i,j} \hat{\mu}_i^{(1)} \hat{\mu}_j^{(2)} \alpha_{ij} = -1; \ \sum_{i,j} \hat{\mu}_i^{(1)} \hat{\mu}_j^{(2)} \beta_{ij} = -1. \tag{18}$$

We obtain

$$\Gamma^{\pm}_{x,-x,z}(R) = \Gamma_0 \left\{ 1 \mp \frac{3}{2} \left(\frac{\sin\{k_0 R\}}{k_0 R} + \frac{\cos\{k_0 R\}}{(k_0 R)^2} - \frac{\sin\{k_0 R\}}{(k_0 R)^3} \right) \right\}, \tag{19}$$

where the subscripts $x,-x,z$ in $\Gamma^{\pm}$ indicate the directions of orientation of dipole 1 and 2, respectively, and that of the separation vector **R**. Consider next the case in which both dipoles are parallel to **R**. Once again we can set **R** along the positive z axis and now assume that both dipoles are also along the positive z axis. This corresponds to $\hat{\mathbf{R}}=(0,0,1)$; $\hat{\boldsymbol{\mu}}^{(1)}=(0,0,1), =\hat{\boldsymbol{\mu}}^{(2)}$, as in Fig. 1(c). We then have

$$\sum_{i,j}\hat{\mu}_i^{(1)}\hat{\mu}_j^{(2)}\alpha_{ij}=0;\ \sum_{i,j}\hat{\mu}_i^{(1)}\hat{\mu}_j^{(2)}\beta_{ij}=-2; \tag{20}$$

and we obtain for this case

$$\Gamma^{\pm}_{z,z,z}(R)=\Gamma_0\left\{1\mp 3\left(\frac{\cos\{k_0R\}}{(k_0R)^2}-\frac{\sin\{k_0R\}}{(k_0R)^3}\right)\right\}. \tag{21}$$

Using the result in Eq. (17) it is easy to show that in the small distance limit we have

$$\Gamma^{+}_{x,-x,z}\approx 0;\ \ \Gamma^{-}_{x,-x,z}\approx 2\Gamma_0 \tag{22}$$

indicating that it is the antisymmetric pair state that is superradiant and the symmetric rate is subradiant. The situation is exactly the same for the second case we considered. We find in the small distance limit,

$$\Gamma^{+}_{z,z,z}(R)\approx 0_0;\ \ \Gamma^{-}_{z,z,z}(R)\approx 2\Gamma_0 \tag{23}$$

indicating that it is the antisymmetric pair state that is superradiant and the symmetric state is subradiant for this case.

The reason for singling out the above set of antiparallel dipole orientations and separation vectors for detailed evaluations will become clear in the following section when we discuss the case of the dipole emitter in the presence of a perfect mirror.

III. THE EFFECTS OF A PERFECT MIRROR

The simplest cavity effects arise in the situation where a perfect conductor occupies the half space $z<0$ and the second half space $z>0$ is a dielectric of dielectric constant ε. The perfect conductor is assumed to exclude all electromagnetic fields from its interior so that the interface at $z=0$ is effectively a perfect mirror to all electromagnetic fields on the dielectric side. A dipole emitter localized in the dielectric can only interact with and via electromagnetic fields satisfying mirror boundary conditions. The quantized electric fields in this case are given by [18]

$$\mathbf{E}(\mathbf{r},t)=\int d^2\mathbf{k}_{\parallel}\int_0^{\infty}dk_z\{a_s(\mathbf{k}_{\parallel},k_z)\boldsymbol{\mathcal{E}}_s(\mathbf{r},t) + a_p(\mathbf{k}_{\parallel},k_z)\boldsymbol{\mathcal{E}}_p(\mathbf{r},t)+\text{H.c.}\}, \tag{24}$$

where $\mathbf{k}_{\parallel}$ is an in-plane wave vector and k_z is a wave vector perpendicular to the interface plane, i.e., along the z axis and we have written $\mathbf{r}=(\mathbf{r}_{\parallel},z)$. $a_{s(p)}$ are the s-polarized (p-polarized) mode annihilation operators and $\boldsymbol{\mathcal{E}}_{s(p)}(\mathbf{r},t)$ are the corresponding electric-field functions which are explicitly given by

$$\boldsymbol{\mathcal{E}}_s(\mathbf{r},t)=C_s(\hat{\mathbf{k}}_{\parallel}\times\hat{\mathbf{z}})\sin(k_zz)e^{i(\mathbf{k}_{\parallel}\cdot\mathbf{r}_{\parallel}-\omega t)}, \tag{25}$$

where $\omega=(k_{\parallel}^2+k_z^2)^{1/2}$ and

$$\boldsymbol{\mathcal{E}}_p(\mathbf{r},t)=C_p\left\{\hat{\mathbf{k}}_{\parallel}\left(\frac{ik_z}{\omega}\right)\sin(k_zz)-\hat{\mathbf{z}}\left(\frac{k_{\parallel}}{\omega}\right)\cos(k_zz)\right\}e^{i(\mathbf{k}_{\parallel}\cdot\mathbf{r}_{\parallel}-\omega t)}, \tag{26}$$

where carets denote unit vectors and $C_{s(p)}$ are mode normalization factors such that the mode functions satisfy the requirement in Eq. (4). Explicitly, we have

$$C_s(k_{\parallel},k_z)=\left(\frac{\hbar c^2}{2(2\pi)^3\varepsilon^2\varepsilon_0k_{\parallel}^2\omega}\right)^{1/2},\qquad C_p(k_{\parallel},k_z)=\left(\frac{\varepsilon_0\varepsilon}{\mu_0}\right)^{1/2}C_s(k_{\parallel},k_z). \tag{27}$$

Direct evaluations for a dipole emitter situated at a distance z from the surface yield the following results for a dipole parallel to the surface ($\Gamma_{\parallel}(z)$) and perpendicular to it ($\Gamma_{\perp}(z)$):

$$\Gamma_{\parallel}(z)=\Gamma_0\left\{1-\frac{3}{2}\left(\frac{\sin 2k_0z}{2k_0z}+\frac{\cos 2k_0z}{(2k_0z)^2}-\frac{\sin 2k_0z}{(2k_0z)^3}\right)\right\}, \tag{28}$$

$$\Gamma_{\perp}(z)=\Gamma_0\left\{1-3\left(\frac{\cos 2k_0z}{(2k_0z)^2}-\frac{\sin 2k_0z}{(2k_0z)^3}\right)\right\}, \tag{29}$$

where, as before, $k_0=\omega_0/c$.

The results in Eqs. (28) and (29) can clearly be interpreted as arising from a correlated state between the real dipole emitter and its mirror image. Since a perfect mirror inverts the signs of the charges, the orientation are as shown in Figs. 1(b) and 1(d), we should be able to ascertain this picture by direct comparison of these results with those in Sec. II of dipoles in unbounded space. It is straightforward to deduce in view of Eqs. (19) and (28) that

$$\Gamma_{\parallel}(Z)=\Gamma^{+}_{x,-x,z}(R=2z)\quad\text{(subradiant)} \tag{30}$$

and in view of Eqs. (21) and (29)

$$\Gamma_{\perp}(Z)=\Gamma^{+}_{z,z,z}(R=2z)\quad\text{(subradiant)}. \tag{31}$$

These results indicate that in both parallel and perpendicular orientations a real dipole selects the symmetric pair state in correlations with its image in the mirror. The other possibility, namely, an antisymmetric correlation state of the dipole with its image does not exist.

In the following two sections, we consider a single dipole emitter and a pair of emitters localized within dielectric regions, either on the same side or on opposite sides of a thin metallic screen separating two different dielectrics. It should be interesting to find out how the image-type correlations described above for the case of a perfect mirror will manifest themselves in the new context and how the correlations evolve with the changing parameters of the structure.

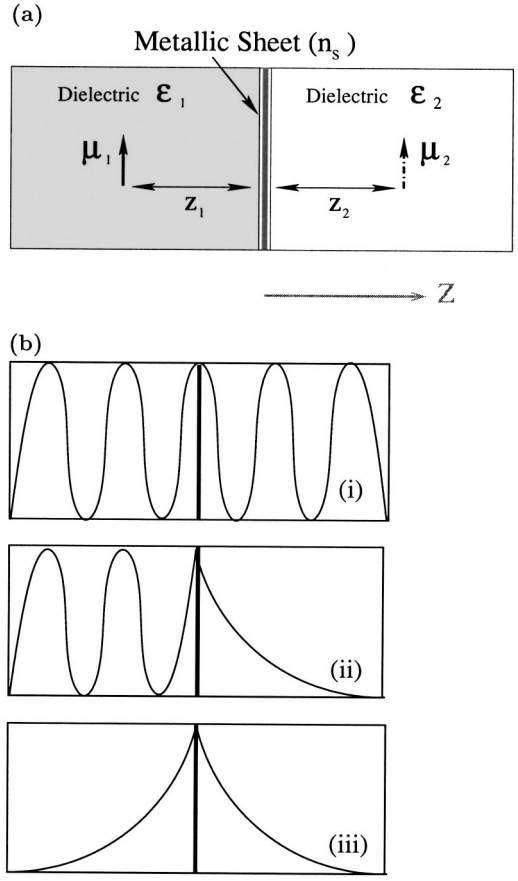

FIG. 2. (a) A schematic figure showing the asymmetric dielectric multilayer cavity comprising two dielectric half spaces of dielectric constants ε_1 and ε_2 separated by a thin metallic sheet with a finite areal electron density n_s. (b) The figure schematically shows the three types of solutions allowed by the asymmetric structure (i) propagating, (ii) evanescent, and (iii) surface modes (schematic).

IV. ASYMMETRIC DIELECTRIC STRUCTURE

The planar microcavity we now use is shown schematically in Fig. 2(a), where ε_1 and ε_2 are different dielectric constants of the homogeneous dielectrics occupying the half spaces $z<0$ and $z>0$, sandwiching a thin metallic film that is characterized by its finite electron density n_s. The film occupies the plane $z=0$ and has a finite conductivity σ at frequency ω, which is given by

$$\sigma = \frac{i n_s e^2}{m^*(\omega + i\gamma)}, \tag{32}$$

where m^* and e are the electronic mass and charge in the metallic film and the small imaginary term $i\gamma$ in the denominator accounts for the plasma loss. The finite conductivity induces an in-plane electric current density $\mathbf{J}_\parallel = \sigma \boldsymbol{\mathcal{E}}_\parallel$ and this affects one of the electromagnetic boundary conditions involving the tangential magnetic-field vector. We have

$$\hat{\mathbf{z}} \times \{\boldsymbol{\mathcal{H}}(z=0_+) - \boldsymbol{\mathcal{H}}(z=0_-)\} = \sigma \boldsymbol{\mathcal{E}}_\parallel(z=0), \tag{33}$$

where $0_\pm = \lim_{\eta \to 0}(\pm \eta)$. The magnetic-field function follows from the electric field using Maxwell's equation:

$$\boldsymbol{\mathcal{H}} = \frac{\boldsymbol{\nabla} \times \boldsymbol{\epsilon}}{i \mu_0 \omega}. \tag{34}$$

In order to determine the mode functions we need the boundary condition in Eq. (33), together with the continuity of the tangential component of the electric field at $z=0$, namely,

$$\boldsymbol{\mathcal{E}}_\parallel(z=0_+) = \boldsymbol{\mathcal{E}}_\parallel(z=0_-). \tag{35}$$

The appropriate field functions are best evaluated using a standard procedure in which a plane wave, which can either be transverse magnetic (TM) or transverse electric (TE) is incident within one of the regions. This is reflected and transmitted at the interface, generating linear combinations of TE and TM solutions in a manner satisfying the above boundary conditions and the procedure is repeated with a plane wave incident within the second region. There are three types of modes emerging from this procedure: (i) propagating modes, which have sinusoidal dependence in both regions of the structure; (ii) evanescent modes, which propagate in one region, but exponentially decay away from the interface in the other region, and (iii) interface modes, which decay exponentially away from the interface in both regions of the structure. Figure 2(b) schematically shows the variations of the three types of mode in the region of the metallic film. The quantized electric field appropriate for the system can be written as follows. For the propagating and evanescent modes, we write

$$\mathbf{E}(\mathbf{r},t) = \sum_{\eta=p,e} \int d^2\mathbf{k}_\parallel \int_0^\infty dk_{z1} \times \{\boldsymbol{\mathcal{E}}(\eta, \mathbf{k}_\parallel, k_{z1}, \mathbf{r}_\parallel, z, t) a_\eta(\mathbf{k}_\parallel, k_{z1}) + \text{H.c.}\}, \tag{36}$$

where η labels the type of mode as either propagating (p) or evanescent (e). $\mathbf{k}_\parallel$ is the wave-vector component parallel to the interface and k_{z1} is a component perpendicular to the interface in region. The corresponding component k_{z2} in region 2 is not an independent variable since it is easy to show that we have

$$k_{z2}^2 = \alpha k_{z1}^2 + (\alpha - 1) k_\parallel^2, \tag{37}$$

where α is the ratio of the dielectric constants,

$$\alpha = \frac{\varepsilon_2}{\varepsilon_1}. \tag{38}$$

Note that k_{z1} and k_{z2} are, in general complex, depending on the type of mode, its in-plane wave-vector component $\mathbf{k}_\parallel$, and its frequency $\omega(k_\parallel, k_{z1})$. For the interface modes, we write

$$\mathbf{E}(\mathbf{r},t) = \int d^2\mathbf{k}_\parallel \{\boldsymbol{\mathcal{E}}_s(\mathbf{k}_\parallel, \mathbf{r}_\parallel, z, t) b_s(\mathbf{k}_\parallel) + \text{H.c.}\}. \tag{39}$$

The vector functions in Eqs. (36) and (39) are obtained analytically, but are unfortunately too complex to display here, which is somewhat surprising in view of the apparent simplicity of the planar structure, albeit asymmetric. The full expressions will be displayed elsewhere [35]. Finally, the operators $a_\eta(\mathbf{k}_\parallel, k_{z1})$ and $b_s(\mathbf{k}_\parallel)$ and their Hermitian conjugates are the mode annihilation and creation opertors satisfying boson commutation relations

$$[a_\eta(\mathbf{k}_\parallel, k_{z1}), a^\dagger_{\eta'}(\mathbf{k}'_\parallel, k'_{z1})] = \delta_{\eta\eta'}\delta(\mathbf{k}_\parallel - \mathbf{k}'_\parallel)\,\delta(k_{z1} - k'_{z1}) \tag{40}$$

and

$$[b_s(\mathbf{k}_\parallel), b_{s'}(\mathbf{k}'_\parallel)] = \delta_{ss'}\delta(\mathbf{k}_\parallel - \mathbf{k}'_\parallel). \tag{41}$$

The deexcitation of quantum states occurs by emission into the three types of modes. Calculations are typically done by evaluating contributions from an individual type of mode and the result for a given situation is the sum of all contributions.

V. DEEXCITATION OF A SINGLE DIPOLE EMITTER

Consider a single dipole emitter localized in the vicinity of the interface that is occupied by the metallic screen. Note that the difference in this system stems partly from the fact that dipole emitters can be localized on either side of the screen. The interaction Hamiltonian is

$$H_{int} = -\boldsymbol{\mu}\cdot\mathbf{E}(\mathbf{r}, t), \tag{42}$$

where $\boldsymbol{\mu}$ is the electric dipole moment vector operator and $\mathbf{E}(\mathbf{r}, t)$ is the full quantized electric-field operator that incorporates local-field corrections in the manner described earlier. The deexcitation rate is given by the Fermi golden rule

$$\Gamma(\mathbf{r}) = \frac{2\pi}{\hbar^2}\sum_{\eta=p,e,s}\sum_{Q}|\langle e;\{0\}|H_{int}|g;\{Q,\eta\}\rangle|^2\,\delta(\omega_0 - \omega(Q,\eta)), \tag{43}$$

where Q represents appropriate mode variables, while $\{0\}$ designates a vacuum state of the given type of mode and $\{Q, \eta\}$ a single-mode state. The evaluations are done analytically, but the results for a given set of parameters proceed using numerical methods. In particular, we can explore variations with the electron density n_s of the metallic sheet and for varying emitter position, both in the near zone and in the far zone of the structure.

Figure 3 displays the variations of the emission rate with the electron density for an emitter fixed at the point $z = 50$ nm. The parameters are such that $\varepsilon_2 = 1$, while ε_1 takes three diffferent values: $\varepsilon_1 = 1$, 2, and 3. The results of this figure show that the relaxation rate exhibits a minimum at low density which can be explained as due to screening arising from the propagating modes. As the density increases, the relaxation rate increases and exhibits a maximum at a density that is characteristic of that emitter position. The rate then decreases as the density further increases,

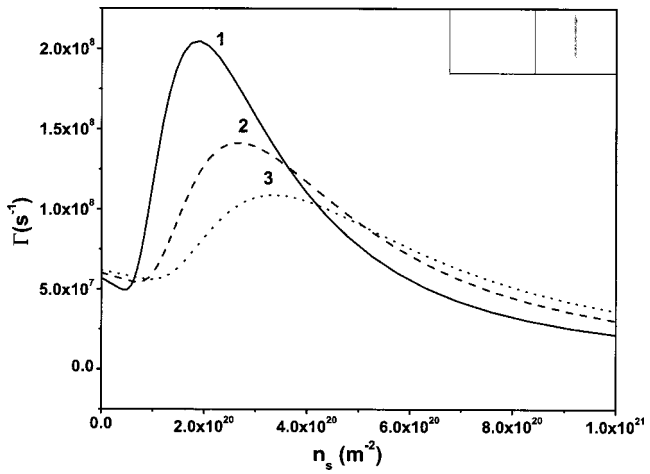

FIG. 3. Variations of the dipole relaxation rate with the electron density n_s for a single dipole emitter of frequency ω_0 such that $\hbar\omega_0 = 2.0$ eV. The emitter is situated at a distance $z = 50$ nm in dielectric 2 (taken to be vacuum where $\varepsilon_2 = 1$) in front of the metallic sheet as an overlayer on three different types of dielectric 1, for which $\varepsilon_1 = 1, 2,$ and 3. See the text for a description of these results.

diminishing to small values. This is consistent with screening expected at much higher electron densities. The large density limit is formally identified as equivalent to a perfect conductor film limit where the metallic film completely screens electromagnetic fields sampled by dipole emitters located on either side of the film.

Figures 4(a) and 4(b) show the variations of the relaxation rate for a dipole emitter oriented parallel to the film plane with the position for (a) a relatively low electron density and (b) a much higher electron density. In Fig. 4(a), the rate variation in the near zone (the region close to the film on both sides) is such that the relaxation process is dominated by emission into the interface mode channel. In the intermediate and far zones, the role of the interface modes is negligible and the dominant role is taken up by emission into the propagating and evanescent mode channels. In Fig. 4(b) where the density is higher than in (a), the contributions from the surface modes are negligible and the rate diminishes to very small values for dipoles located at or near the film on both sides. The continuity of the emission rate at the screen indicates that at this high density the film is practically perfectly conducting. There is perfect screening, but the situation close to the film is not the same as that of a dipole in front of a perfectly conducting half space. The variations in the far zone for this high density suggest that image effects are dominant for dipole positions further away from the screen on both sides. At dipole positions far removed from the screen on either side we recover the result $\Gamma_0(\varepsilon)$ that is appropriate for the unbounded dielectric in which the dipole is located.

Figure 5 shows the changes in the emission rate with position for a dipole oriented parallel to the film plane and for different values of ε_1, illustrating the influence of dielectric mismatch. For a fixed $\varepsilon_2 = 1$, we see how the emission rate is modified for an emitter localized on a given side of the

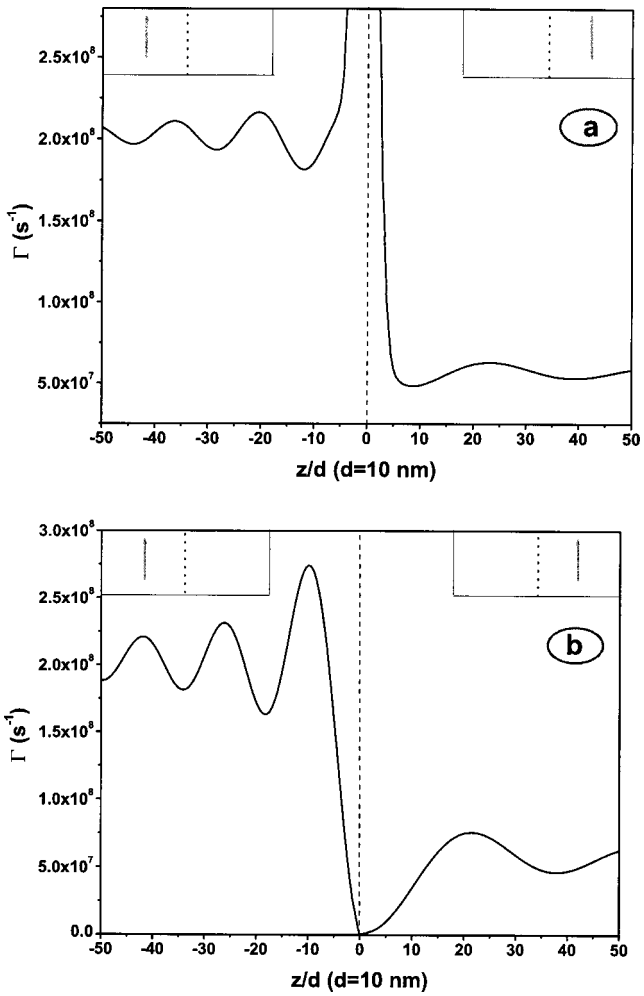

FIG. 4. Variations of the emission rate with dipole position for a dipole of frequency ω_0 such that $\hbar\omega_0=2.0$ eV. The film electron density is (a) $n_s=1.7\times10^{20}$ m^{-2} and (b) $n_s=6.5\times10^{21}$ m^{-2}. The dielectric constants are taken to be $\varepsilon_1=4$ and $\varepsilon_2=1$ in both cases. See text for a discussion on the results.

film as ε_1 is increased. The effects of the film (albeit, at a low density in Fig. 5) manifest themselves partly in the lack of symmetry with respect to the screen. On the right-hand side, we see that the rate changes very little with increasing ε_1 and this can be attributed to screening at low densities due to the presence of the film.

VI. PAIR CORRELATIONS

The investigation of pair correlations follows the steps in Sec. III. Once again Eq. (13) is the starting point, but with the modes appropriate for the asymmetric structure. The procedure is largely analytical, albeit quite complicated on account of the complicated forms of the mode functions. The results can be written in a form analogous to Eq. (14);

$$\Gamma^{\pm}(\mathbf{r}_1,\mathbf{r}_2)=\frac{1}{2}\{\Gamma_0(\mathbf{r}_1)+\Gamma_0(\mathbf{r}_2)\}\pm\sum_{i,j}\hat{\mu}_i^{(1)}\hat{\mu}_j^{(2)}\Gamma_{ij}(\mathbf{r}_1,\mathbf{r}_2), \tag{44}$$

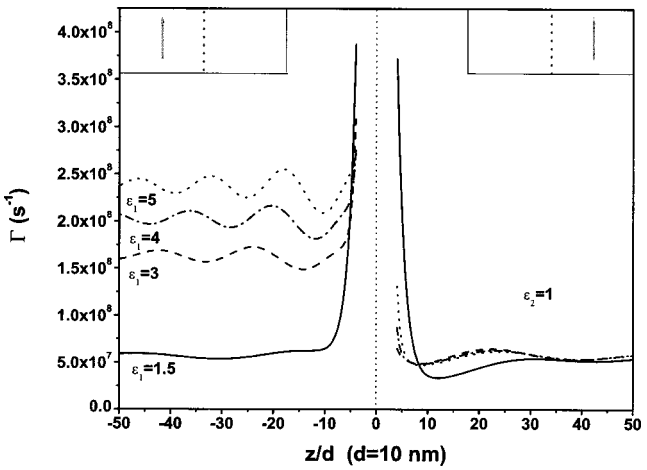

FIG. 5. Variations of the emission rate with position for a dipole of frequency ω_0 such that $\hbar\omega_0=2.0$ eV. The dipole moment vector is oriented parallel to the film plane and the electron density is $n_s=1.7\times10^{20}$ m^{-2}, $\varepsilon_2=1$, and for different values of ε_1, illustrating the influence of dielectric mismatch.

where $\Gamma_0(\mathbf{r}_1)$ and $\Gamma_0(\mathbf{r}_2)$ are the individual emission rates at the points where the dipole emitter 1 and dipole emitter 2 are localized, respectively. $\hat{\mu}_i^{(1)}$ and $\hat{\mu}_j^{(2)}$ are the ith and the jth Cartesian vector components of unit vectors in the direction of the dipole moments of emitters 1 and 2, respectively. Γ_{ij} are simultaneous functions of the the emitter positions. Unfortunately, even for the simplest cases, these analytical functions are too complicated to be displayed here. Meaningful results are obtained with the help of numerical techniques. It is useful to select a few special cases for illustration purposes and, as we shall see, this is reasonably effective in uncovering interesting trends.

Figure 6 shows the variations of the $\pm$ emission rates for a pair of emitters with dipole vectors oriented parallel to the metallic sheet plane. In Fig. 6(a) dipole 1 is fixed, in the near zone at $z_1=-20$ nm, while the position of dipole 2 varies across the sheet from left to right. The parameters are such that $\varepsilon_1=2.0$; $\varepsilon_2=1$; and metallic sheet density $n_s=1.7\times10^{20}$ m^{-2}. The dipole oscillation frequency is such that $\hbar\omega_0=2.0$ eV. There are three interesting observations here. First, we note the strong enhancement in the near zone when dipole 2 is close to the surface on both sides of the screen. Second, when the position of dipole 2 coincides with that of dipole 1, on the left of the screen, we get the expected super-radiance for Γ^+ and subradiance for Γ^-. However, identical behaviors can be seen when the position of dipole 2 is at the image position $z_2\approx+20$ nm, i.e., to the right of the screen. We deduce from this that there are super-radiance and subradiance phenomena displayed by image-type effects. At the point $z_2=20$ nm, dipole 2 and the image of dipole 1 coincide in position. The real dipoles are parallel, but at the image position dipole 2 and the image of dipole 1 they are antiparallel and we get super-radiance for Γ^+ and subradiance for Γ^- at this position in this near-zone situation.

Figure 6(b) shows the corresponding near-zone variation for antiparallel dipoles, both perpendicular to the film plane, as shown by the two insets to Fig. 6(b). At the image posi-

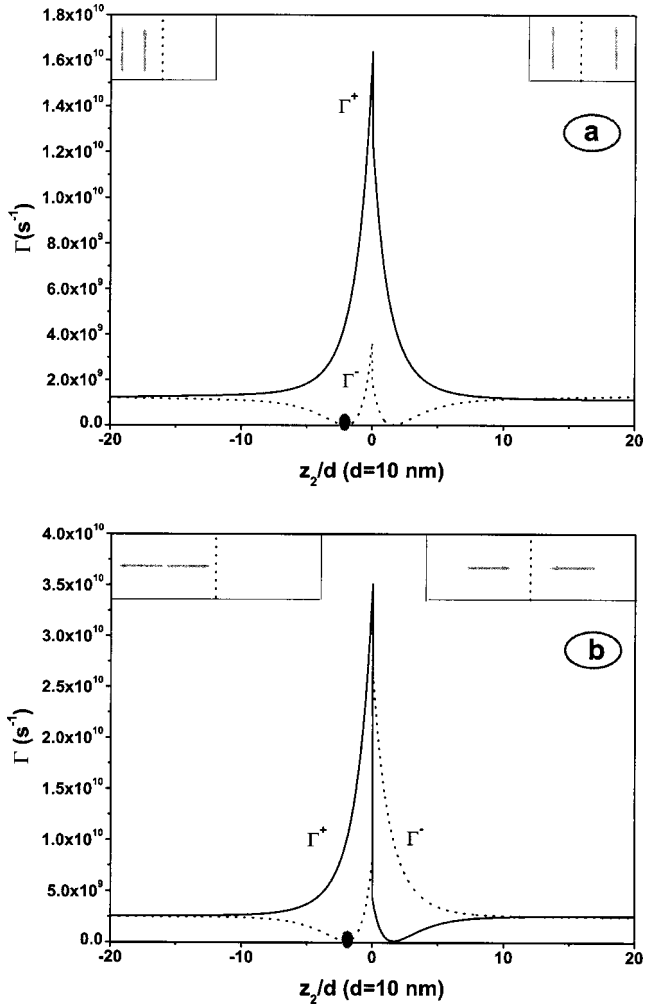

FIG. 6. (a) Cooperative rates $\Gamma^{\pm}$ in the near zone. Here dipole 1 is fixed at $z_1=-20$ nm in region 1, where $\varepsilon_1=2$. Dipole 2 changes position from the left of the screen in region 1 to the right of the screen in region 2, where $\varepsilon_2=1$. Here the dipoles are both parallel to interface as shown in the insets of the figure. The density of the film is $n_s=1.7\times10^{20}$ m^{-2}; (b) the corresponding situation for antiparallel dipoles. See the text for further discussions on the results.

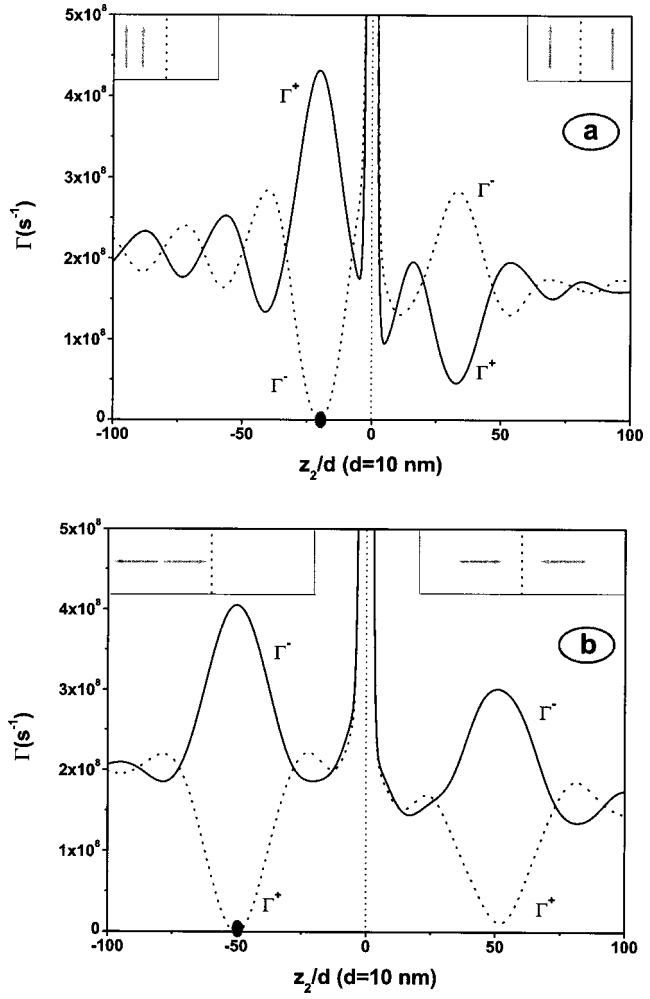

FIG. 7. (a) The cooperative rates $\Gamma^{\pm}$ in the far zone for the case $\varepsilon_2=1$ and $\varepsilon_1=4$. The two dipoles are both parallel to the film plane and oscillation frequency ω_0 such that $\hbar\omega_0=2.0$ eV and the density is $n_s=1.7\times10^{20}$ m^{-2}. Dipole 1 is fixed at $z_1=-200$ nm and dipole 1 changes position across the screen; (b) here the dipoles are antiparallel and both are perpendicular to the film plane with dipole 1 fixed at $z_1=-500$ nm. See text for a discussion on these results.

tions, the situation is a super-radiance for Γ^- and a subradiance for Γ^+. This behavior is opposite to that in Fig. 6(a) and is consistent with the manner in which a real dipole selects the appropriate correlation pair symmetry with an image, discussed in the perfect conductor half-space case in Sec. III.

Figure 7(a) shows the situation in the far zone. Here, dipole 1 is fixed at the position $z_1=-200$ nm and dipole 2 varies in position across the screen. When dipole 2 is far to the left or far to the right, the dipole system displays oscillations with distance, which are consistent with a dipole pair in free space. This interpretation can be confirmed by comparing a period of these oscillations with a transition wavelength $\lambda_0=2\pi/k_0$. In the region where dipole 1 is fixed, we see that super-radiance and subradiance effects are exhibited by Γ^+ and Γ^-, respectively. However, on the right-hand side, the situation is reversed: Γ^- shows super-radiance and Γ^+ subradiance. This behavior can be explained in terms of correlation between dipole 2 and the image of dipole 1 at $z_2=+200$ nm. Note, however, that Γ^+ is not exactly zero at $z_2=+200$ nm. This can be traced to the effects of a finite electron density. We have checked that as the density increases, the super-radiance behavior $\Gamma^+(z_2=200$ nm) vanishes for the case in Fig. 7(a).

Figure 7(b) shows the situation as in Fig. 7(a), but for antiparallel dipoles that are both perpendicular to the film plane, as shown in the two insets of the figure. In this case, there is complete reversal in behavior due to image and dipole orientation effects. In the left region where dipole 1 is fixed, we see super-radiance for Γ^- and subradiance from Γ^+ when the two dipoles coincide in position. When dipole 2 crosses the film to the right-hand side, we find Γ^- is superradiant there too and Γ^+ is subradiant. Note that the image position is not exactly at $+500$ nm due to the finiteness of the density n_s and the fact that $\varepsilon_1=4$ in this case.

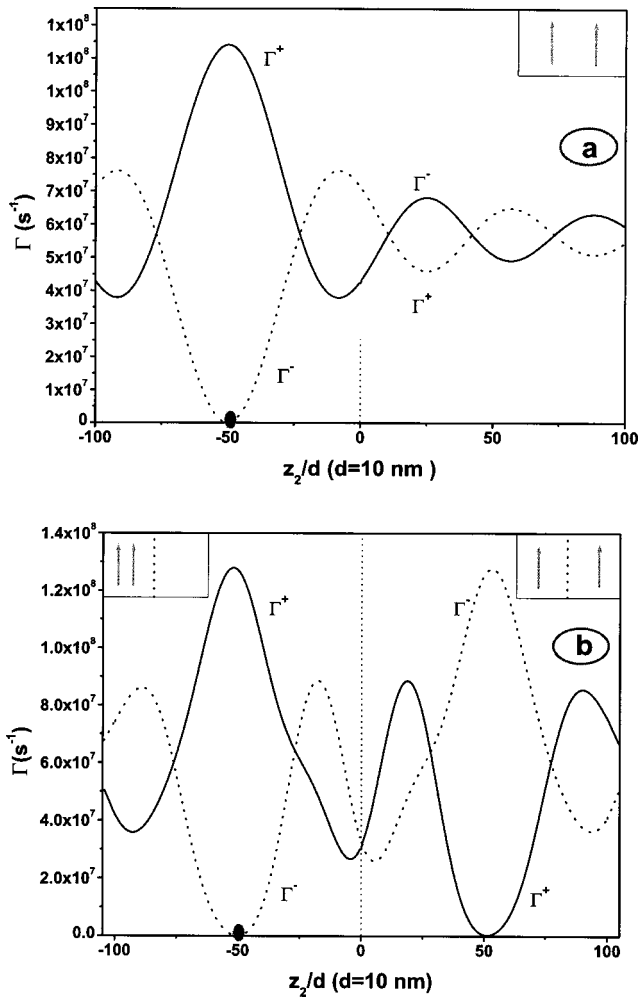

FIG. 8. The case of a homogeneous dielectric $\varepsilon_1=\varepsilon_2$. Here we have two dipoles, both parallel to the film plane, with dipole 1 fixed at $z_1=-500$ nm and the position z_2 of dipole 2 varies across the $z=0$ plane: (a) the limit of very low density $n_s=7.3\times10^{16}$ m^{-2}; (b) a much higher density $n_s=6.5\times10^{21}$ m^{-2}. See text for a discussion on these results.

Figure 8(a) displays the two-dipole emission rates arising from our general theory in the limit $n_s\to0$ and $\varepsilon_1=\varepsilon_2$, with the dipoles oriented parallel to the film plane. With the film essentially absent due to diminished electron density and the two half spaces filled by the same material, the $z=0$ plane is now simply an arbitrary coordinate plane. The result is seen to coincide with that emerging from the case of a dipole pair immersed in a homogeneous dielectric.

Figure 8(b) shows the result of the same situation as in Fig. 8(a), but this time corresponds to the large density limit (the perfect conductor film limit is formally given as $n_s\to\infty$). Note the apparent symmetry of the situation gives rise to unusual image-type effects in this far zone. With dipole 1 fixed at $z_1=-500$ nm, the usual super-radiance and subradiance effects are seen to arise when dipole 2 is in the same region as dipole 1. When dipole 2 crosses the film and enters the region on the right, it exhibits the reverse effects. At image positions we see that Γ^- is super-radiant at the image 1 position (at $z_2=+500$ nm), while Γ^+ is exactly subradiant. This figure should be compared with Fig. 7(a) where the density is smaller.

VII. COMMENTS AND CONCLUSIONS

In this paper, we have considered quantum correlations in dielectric cavity QED and presented analytical accounts and corresponding results for a number of situations, including pair correlations in unbounded space and single-dipole correlations with its image inside a perfect mirror in the form of a perfect conductor half space.

We have also demonstrated that different forms of quantum correlation occur in the context of a planar asymmetric dielectric cavity involving a metallic screen, separating two different dielectrics. We have seen that correlations arise for a single dipole with its quasiimage on either side of the metallic screen and the correlations are influenced significantly by the magnitude of the electron density of the metallic film, together with dielectric mismatch and dipole orientation. We have seen that the situation in the case of our thin metallic film is quite different from that in the case of a half space [36,37]. The results for correlations in front of a half-space metal of finite conductivity, such as that considered by Morawitz and Philpott [36], can in fact emerge from a system similar to ours, but with a finite-thickness metallic layer replacing our thin metallic screen. In the limit of large metallic layer thickness one should then recover results for a half-space system.

We have seen that quantum correlations can arise for a dipole pair when both are localized on the same side of the screen or on different sides across the screen. Correlations across the screen are particularly intriguing as the dipoles influence each other to an extent depending on the parameters of the system. Image-type effects of a complicated nature are exhibited, depending on the magnitude of the density of the metallic screen, dipole orientation, and dielectric mismatch. At low densities, the two dipoles on different sides of the screen exhibit direct correlations in the near zone as well as the far zone. At sufficiently high densities, screening effects dominate, but the situation for the two-dipole system too is quite distinct from the parallel case of a perfect conductor half space. The super-radiance and subradiance effects which are normally the preserves of symmetric $(+)$ and and antisymmetric $(-)$ quantum states are partially reversed for parallel dipoles and completely reversed for perpendicular dipole correlations across the screen.

The results of this paper should be amenable to experimental verification using the monolayer assembly technique [32] that has been used in recent experiments on surface phenomena [38-40]. The technique facilitates the depositing of molecular dipole active layers at precisely adjustable distances from a metallic film with well-defined electron density. The quantum correlation effects predicted in this paper should be evident in measured fluorescence of the system.

ACKNOWLEDGMENTS

M. Al-Amri is grateful to King Khalid University, Abha, Saudi Arabia for financial support.

[1] M. Bayer, F. Reinecke, F. Weidner, A. Larionov, A. McDonald, and A. Fochel, Phys. Rev. Lett. **86**, 3168 (2001).
[2] V. Giovannetti, P. Vitali, P. Tombesi, and A. Ekert, Phys. Rev. A **62**, 032306 (2000).
[3] *Quantum Computing*, edited by S. L. Braunstein (Wiley-VCH, Berlin, 1999).
[4] *Scalable Quantum Computers*, edited by S. L. Braunstein and K.H. Lo (Wiley-VCH, Berlin, 2001).
[5] G. Brennen and I. Deutsch, Phys. Rev. A **61**, 062309 (2000).
[6] *Cavity Quantum Electrodynamics*, edited by P. Berman (Academic, Amsterdam, 1994).
[7] S. Haroche, in *Fundamental Systems in Quantum Optics*, Les Houches Lectures, Session 53, edited by T. Dalibard, J. Raimond, and Zinn-Justin (North-Holland, Amsterdam, 1992).
[8] Y. Yamamoto and R. Slusher, Phys. Today **46** (6), 66 (1993).
[9] W.L. Barnes, J. Mod. Opt. **45**, 661 (1998).
[10] H. Rigneault, S. Robert, C. Begon, B. Jacquier, and P. Morett, Phys. Rev. A **55**, 1497 (1997).
[11] I. Abram, I. Robert, and R. Kuszelewicz, IEEE J. Quantum Electron. **34**, 71 (1998).
[12] P. Burrows, V. Khalfin, G. Gu, and S.R. Forrest, Appl. Phys. Lett. **73**, 435 (1998).
[13] S. Robert, H. Rigneault, and F. Lamarque, J. Opt. Soc. Am. B **15**, 1773 (1998).
[14] F. Cairo, F. De Martini, and D. Murra, Phys. Rev. Lett. **70**, 1413 (1993).
[15] F. Fainstein, B. Jusserand, and V. Thierry-Mieg, Phys. Rev. Lett. **75**, 3764 (1995); Phys. Rev. B **53**, R13 287 (1996).
[16] R.L. Hartman and P.T. Leung, Phys. Rev. B **64**, 193308 (2001).
[17] E.A. Hinds, Adv. At., Mol., Opt. Phys. **28**, 237 (1991).
[18] G. Barton, J. Phys. B **7**, 2134 (1974).
[19] P.W. Milonni and P.L. Knight, Opt. Commun. **9**, 119 (1973).
[20] M. Babiker, J. Phys. A **9**, 799 (1976).
[21] A. Kamli and M. Babiker, Phys. Rev. A **62**, 043804 (2000).
[22] R.H. Dicke, Phys. Rev. **93**, 99 (1954).
[23] C.R. Bennett, J.B. Kirk, and M. Babiker, Phys. Rev. A **63**, 063812 (2001).
[24] C.R. Bennett, M. Babiker, and J.B. Kirk, J. Mod. Opt. **49**, 269 (2002).
[25] C.R. Bennett, J.B. Kirk, and M. Babiker, Phys. Rev. A **63**, 033405 (2001).
[26] S.M. Barnett, in *Quantum Fluctuations*, Les Houches Lectures, Session 62 edited by S. Reynaud, E. Giacobino, and Zinn-Justin (North-Holland, Amsterdam, 1997).
[27] R.J. Glauber and M. Lewinstein, Phys. Rev. A **43**, 467 (1991).
[28] P. de Vries and A. Lagendijk, Phys. Rev. Lett. **81**, 1381 (1998).
[29] G. Juzeleunas and D.L. Andrews, Adv. Chem. Phys. **112**, 357 (2000).
[30] H.F. Hameka, J. Chem. Phys. **41**, 2006 (1964).
[31] R.H. Lehemberg, Phys. Rev. A **2**, 889 (1970).
[32] R. Mclone and E.A. Power, Mathematika **11**, 91 (1964).
[33] E.A. Power and T. Thirunamachandran, Am. J. Phys. **46**, 370 (1978).
[34] L. Gomberoff and E.A. Power, Proc. R. Soc. London, Ser. A **88**, 476 (1966).
[35] M. Al-Amri, Ph.D. thesis, The University of York, England (unpublished). An electronic copy of the thesis, once completed, will be made available in the Los Alamos Archive.
[36] H. Morawitz and M.R. Philpott, Phys. Rev. B **10**, 4863 (1974).
[37] R.R. Chance, A. Prock, and R. Silbey, J. Chem. Phys. **60**, 2184 (1974); **60**, 2744 (1974); Adv. Chem. Phys. **37**, 1 (1978).
[38] K.H. Drexhage, in *Progress in Optics XII*, edited by E. Wolf (North-Holland, Amsterdam, 1974), p. 165.
[39] R.M. Amos and W.L. Barnes, Phys. Rev. B **55**, 7249 (1997).
[40] P.T. Worthing, R.M. Amos, and W.L. Barnes, Phys. Rev. A **59**, 865 (1999).